UNIVERSITEIT·STELLENBOSCH·UNIVERSITY
jou kennisvennoot • your knowledge partner

An axial flux magnetically geared PM wind generator
(repository copy)

Article:

An Axial Flux Magnetically Geared Permanent Magnet Wind Generator

Rong-Jie Wang*a
Lodewyk Brönn**
Stiaan Gerber*
Pushman Tlali*

This paper presents the design, construction, and experimental performance evaluation of an axial flux magnetically geared permanent magnet (MGPM) machine for wind power application. The optimum electromagnetic design for both magnetically coupled and decoupled configurations is described. Considering the complex structure of the axial flux MGPM machine, special attention is also paid to the mechanical design aspects. The optimized results show that a torque density in excess of $100\,\mathrm{kNm/m^3}$ could be achieved for the active gear part. The inherent overload protection of the MGPM machine has also been demonstrated. Furthermore, the design-related aspects and issues are analyzed and discussed in detail in an attempt to outline problem areas in the design process. Relevant discussions are given and conclusions are drawn. © 2015 Institute of Electrical Engineers of Japan. Published by John Wiley & Sons, Inc.

Keywords: axial field, permanent magnet machine, magnetic gears, wind generator

1. Introduction

The foreseeable energy challenges and the growing environmental concerns are the driving force behind the current worldwide renewable energy development. Among others, wind energy has been identified as a major renewable energy resource. The mainstream drive train of a large wind turbine system has been the doubly fed induction generator (DFIG) with a partially rated power converter that employs a mechanical gearbox to match the speeds between the turbine and DFIG. However, according to the statistics of wind power systems, gearbox failures have been the main cause for downtime, maintenance, and loss of generation revenue [1,2].

In recent years, there has been a renewed interest in magnetic gear (MG) technology as a result of innovations in the design and progress in magnetic materials [3]. Magnetic gears hold several advantages over their mechanical counterparts such as contactless power transfer, inherent overload protection, quiet operation, improved reliability, and low maintenance. Research and developments in MGs have revealed several novel designs of electrical machines [4–6], which elegantly integrate an MG with a traditional PM machine and offer ultrahigh torque/power density. The potential application areas of this technology includes electrical traction drives [6–8] and wind power generation [9,10].

This paper presents the design, mechanical construction, and experimental evaluation of a novel axial flux magnetically geared PM (MGPM) machine for wind power application. Figure 1 shows the mechanical layout of an axial flux MGPM machine. The selection of the axial flux configuration for this research is due to the novelty of this topology and the easy access to both motion components for experimental evaluation. There has not been any published work on the axial flux MGPM machines; thus, ours is likely the first attempt to design, build, and experimentally evaluate this type of machine.

a Correspondence to: Rong-Jie Wang. E-mail: rjwang@ieee.org

* Department of Electrical and Electronic Engineering, Stellenbosch University, Private Bag X1, Matieland 7602, South Africa

** Adventure Power, Wilsonia, East London 5274, South Africa

In the following text, the drive train configuration of a magnetically geared wind generation system, gear ratio selection, and machine topologies are described in Section 2. The design methodology and finite element (FE)-based steady-state performance calculation of the MGPM machine are presented in Section 3. Section 4 gives details of the mechanical design aspects. The experimental investigation of the prototype is presented in Section 5. Relevant discussions are given and conclusions are drawn.

2. Axial Flux MGPM Wind Generation System

The basic drive train configuration of an MGPM wind generator system is shown in Fig. 2, which consists of a wind turbine, an integrated MGPM synchronous generator, and a full-scale power converter. For this particular project, the turbine specifications for a site at the South African Antarctic research base SANAE IV were used. Figure 3 shows the power versus speed curves of the wind turbine for various wind speeds at the specific site. It can be seen that the rated turbine speed for the site is 150 rpm, which is the rated input speed at the low-speed (LS) side of the MGPM machine.

2.1. Selection of gear ratio The gear ratio G_r of the magnetic gear is a function of the number of pole pairs on the high- and low-speed rotors (p_H and p_L) and the number of modulation pieces q_m [3]. For the sake of cost saving, an existing six-pole axial flux stator shown in Fig. 4 is utilized. The technical specifications of the stator are given in Table I.

With the number of high-speed (HS) pole pairs chosen to match the stator pole pairs ($p_H = 3$), and the number of pole pairs on the LS rotor p_L remaining to be chosen, the gear ratio can be calculated by

$$G_r = \frac{p_L}{p_H} = -\frac{n_H}{n_L} \qquad (1)$$

where n_H and n_L are the rotation speeds of the HS and LS rotors, respectively. The minus sign indicates that two rotors rotate in
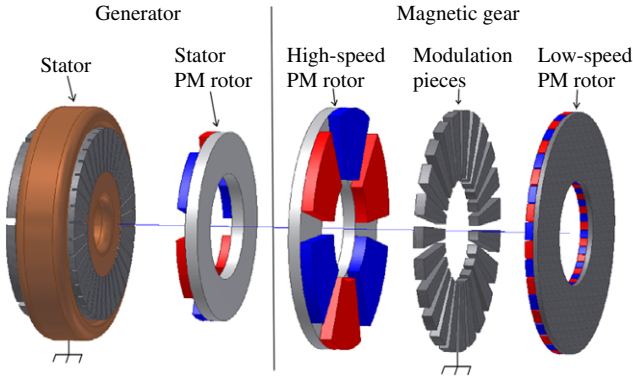
Fig. 1. Mechanical layout of an axial flux MGPM machine
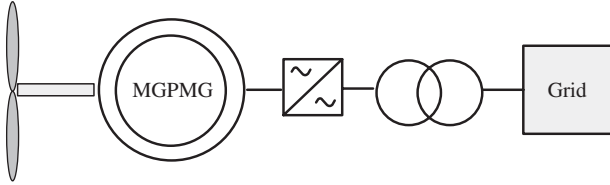

Fig. 2. Drive train configuration of a MGPM wind turbine generator system

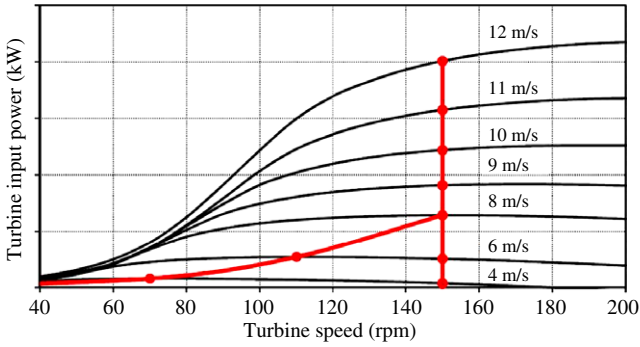Fig. 3. Turbine curves for different wind speeds

Fig. 4. Axial flux stator used for MGPM machine

Table I. Technical specifications of the axial flux stator

Parameters	Values
Power rating (kW)	4
Outer diameter (mm)	250
Inner diameter (mm)	140
Axial length (mm)	58.8
Number of poles	6
Number of stator slots	36
Number of coils per phase	12
Number of turns per coil	27
Parallel wires per conductor	3
Wire size (mm)	0.9
Phase connection	Star
Stator winding layout	double layer

opposite directions. The number of modulation pieces q_m can be determined by

$$q_m = p_L + p_H \qquad (2)$$

For wind power application, the cogging torque has a negative impact on the start-up of the turbine. To check the severity of the cogging torque, a cogging factor f_c expressed by (3) is introduced in [11], which serves as an indication of the amplitude of the cogging torque.

$$f_c = \frac{2pq_m}{N_c} \qquad (3)$$

where N_c is the least common multiple (LCM) between the number of poles on one of the PM rotors p and the number of modulation pieces q_m. From (3) it can be observed that the larger the LCM, the smaller the f_c and thus the smaller the cogging torque. For the lowest cogging torque, a unity cogging factor is preferred. Figure 5 illustrates the relationship between the gear ratio and key gear parameter combinations for $p_H = 3$. Assuming $p_L = 20$, the gear ratio according to (1) is $G_r = 6.67$. For a rated input speed $n_L = 150$ rpm, the HS rotor speed is thus $n_H = 1000$ rpm, resulting in an electrical frequency of 50 Hz. Using (2), the number

of modulation pieces is calculated as $q_m = 23$. The cogging factor $f_c = 1$ in this case.

From Fig. 5, it can also be observed that the lowest cogging factor is associated with fractional gear ratios. This is in good agreement with [10], in which the authors concluded that fractional gear ratios offer the best performance for wind power applications.

2.2. Magnetic circuit configurations For an integrated MGPM machine, there are two possible design configurations, in which the magnetic circuits of the gear part and the machine part could be either decoupled or coupled. For the magnetically coupled topology, magnetic flux goes through all three air gaps and the PMs on the LS rotor contribute to the total flux linkage in the stator. Figure 6 shows the magnetic field distribution in an MGPM machine with magnetically decoupled and coupled topologies.

3. Design procedure

In this section, the electromagnetic design and optimization procedure for the axial flux MGPM machine are described. A hybrid field-circuit design approach is adopted, which consists of a finite element method (FEM) program, a Visual Basic script for creating an FEM model, and an external Python script performing post-processing analysis. The FEM program calculates the total flux
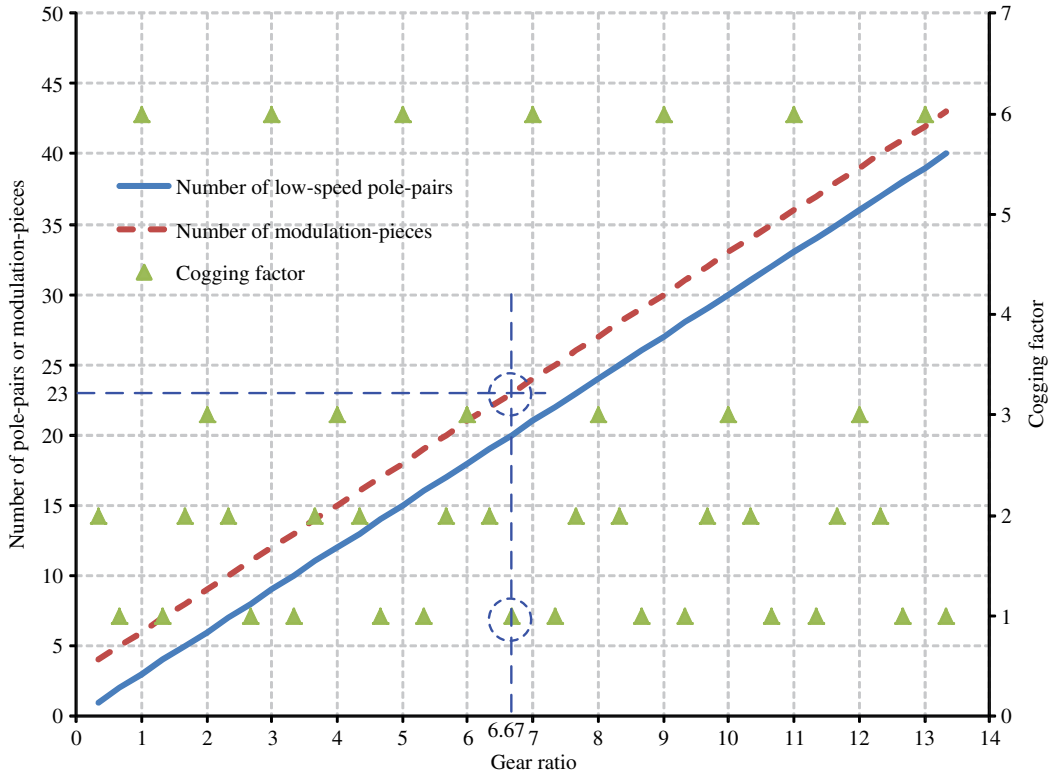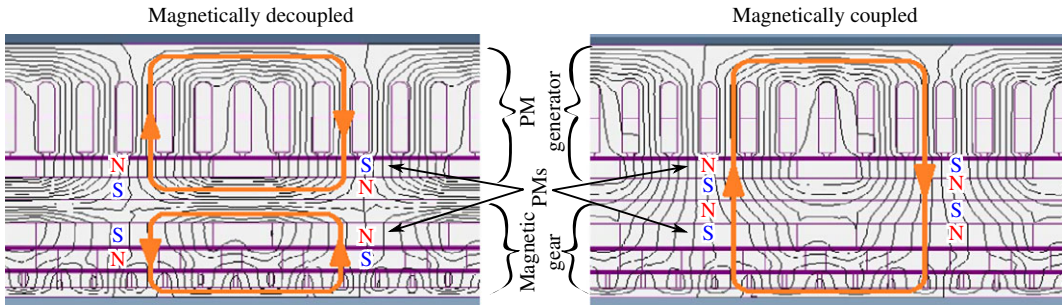
Fig. 5. Selection of gear ratio ($p_H = 3$)

Fig. 6. Magnetic field distribution in an MGPM machine with magnetically decoupled and coupled topologies

linkages of each phase and the relevant forces/torques on the different components of the machine. The external script is then used to conduct further calculations on the results obtained from the FEM program. Figure 7 shows the flowchart of the performance calculation process. The particle swarm optimization (PSO) algorithm, a population-based stochastic optimization technique, was employed to optimize the design. PSO shares many similarities with evolutionary computation techniques (e.g. genetic algorithms) and shows better computational efficiency [12].

3.1. 2D FEM model   For 2D FE modeling, it is a normal practice to represent the axial flux machine as a linear machine. Figure 8 illustrates the linearized layout and the design variables of the axial flux MGPM machine. Typically, an MGPM machine has no electromagnetic symmetry requiring the full FE model of the machine. Figure 9 shows the full FE model and flux plot of the MGPM machine at a certain timestep. In order to use the FEM model in conjunction with an optimization algorithm, the model needs to be generic, which means that the input parameters such as the dimensions and the material properties need to be changeable. This has been implemented with a Visual Basic (VB) script that creates and simulates the FE model and exports the results to the post-processing program.

3.2. Equivalent circuits of the machine   For the performance calculation of the MGPM machines, it is necessary to consider their equivalent circuits. Figure 10 shows the per-phase equivalent circuits for both magnetically coupled and decoupled MGPM machines. For the decoupled topology (Fig. 10(a)), E_1 is the electromotive force (EMF) induced in the stator windings due to the fundamental air gap PM flux linkages of the HS rotor, L_m is the stator main inductance, L_e is the stator end-winding leakage inductance, R_s is the stator resistance, and I_s and V_s are the phase current and voltage, respectively. The shunt resistance R_c is the core loss resistance. The portion of the circuit enclosed by the dashed lines can be directly computed by FEM program. The FE results are then fed into the circuit analysis. For the coupled topology (Fig. 10b), the PMs of the LS rotor also contribute to the total PM flux linkage λ_{pm} in the stator [9], i.e.

$$\lambda_{pm} = \lambda_{pm1} + \lambda_{pm2} \tag{4}$$

Thus a secondary EMF source E_2 is introduced in the equivalent circuit for the coupled topology.

An efficient field-circuit analysis approach for axial flux PM machines presented in [13] is applied for the generator's performance calculations in the design procedure.
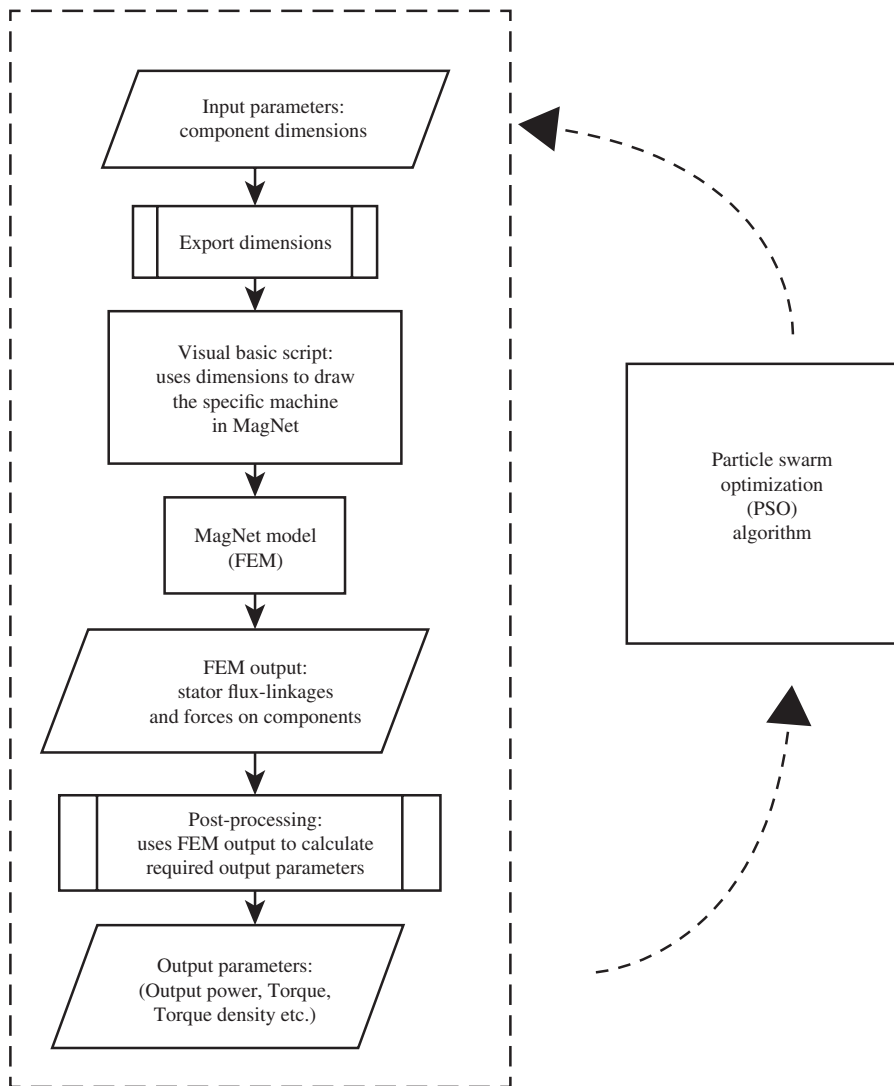
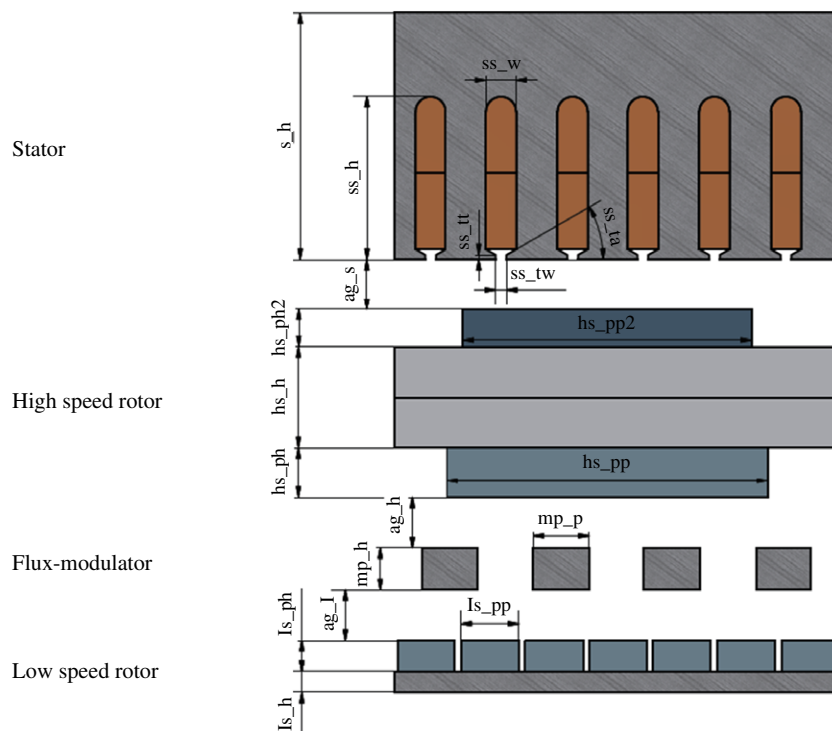Fig. 7. Flowchart of the field-circuit performance calculation of the MGPM machine

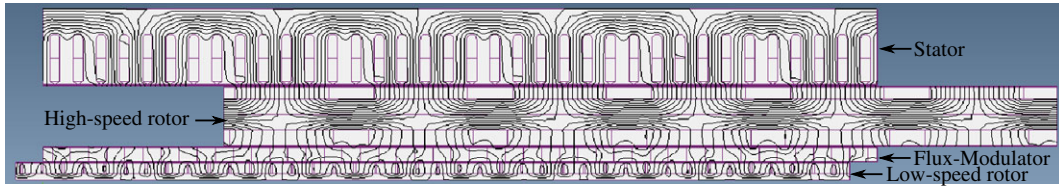Fig. 8. Design variables and FE model layout of the axial flux MGPM machine

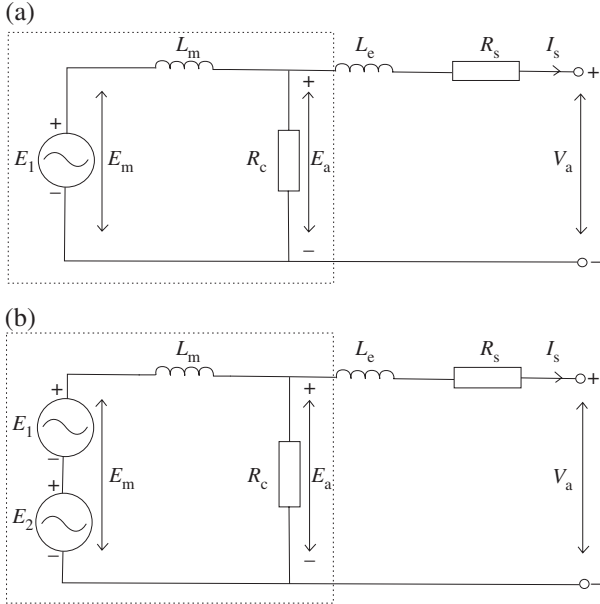Fig. 9. Full FE model and flux plot of the MGPM machine at a certain timestep

Fig. 10. Per-phase equivalent circuits of both a magnetically (a) decoupled and (b) coupled MGPM machine

3.3. Design optimization For the optimal design of an MGPM machine, an inherent constraint must be satisfied, i.e. the rated torque provided by the gear should match the rated torque required on the generator side. The net torque on the HS rotor is zero under steady state. Any sizing mismatch between the gear and the machine leads to an inferior design. Figure 11 shows the relationship between the input torque and the corresponding output power for the axial flux generator. It can be seen that to generate

Table II. Optimization results of the MG with the same diameter as the PM generator

Machine Parameters	Constraints	Optimum
LS rotor height (ls_h) (mm)	$5 \leq ls_h \leq 20$	5
LS pole height (ls_{ph}) (mm)	$4 \leq ls_{ph} \leq 20$	12
LS pole pitch (ls_{pp})	$0.7 \leq ls_{pp} \leq 0.95$	0.8
MP height (mp_h) (mm)	$10 \leq mp_h \leq 30$	10
HS rotor height (hs_h) (mm)	$20 \leq hs_h \leq 30$	30
HS pole height (hs_{ph}) (mm)	$4 \leq hs_{ph} \leq 12$	12
HS pole pitch (hs_{pp})	$0.4 \leq hs_{pp} \leq 0.9$	0.9
Air gap length (mm)	2	–
Objective: Maximize ()	–	–
HS torque (T_{HS}) (Nm)	$T_{HS} \geq 50$	24.43

4 kW power, the input torque on the HS rotor should be about 50 Nm.

An interesting observation is that the optimized gear torque only reaches 50% of the required torque if the gear diameter is kept the same as that of the generator (as shown in Table II). This is largely due to the mismatch between the gear torque and electromagnetic torque on the generator side, which has also been described in [14]. Thus the outer diameter of the gear is another design variable for axial flux MGPM machines. In the final design (see Table III), the outer diameter for the gear part and the generator part are 320 and 250 mm respectively. Table IV summarizes the optimized performance of the MGPM machine.

4. Mechanical Design Considerations

To design an effective renewable energy converter involves not only electrical performance design but also mechanical strength
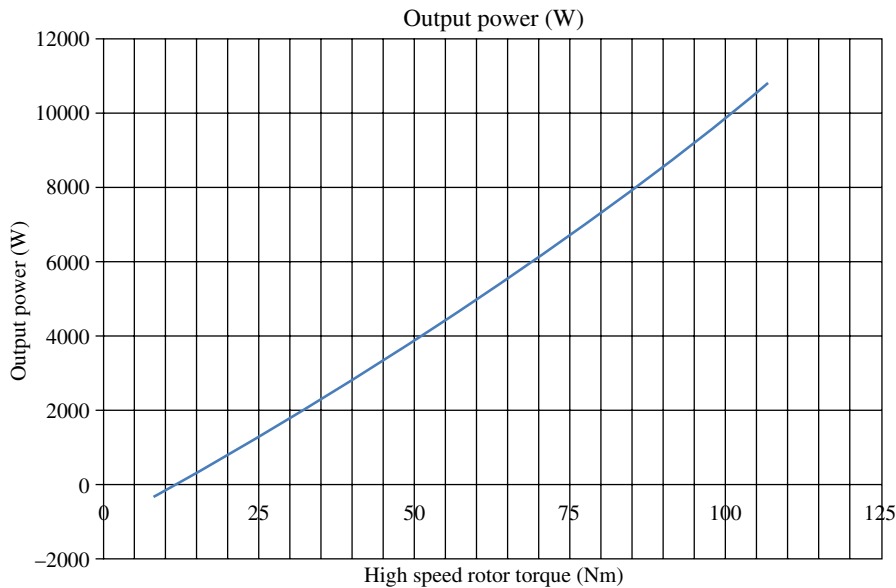

Fig. 11. Output power as a function of HS rotor input torque

Table III. Optimization results of the MG with the gear diameter larger than that of PM generator

Machine parameters	Constraints	Optimum
Outer diameter (D) (mm)	$250 \leq D \leq 330$	320
Inner diameter (d) (mm)	$100 \leq d \leq 140$	140
LS rotor height (ls_h) (mm)	$5 \leq ls_h \leq 20$	5
LS pole height (ls_{ph}) (mm)	$4 \leq ls_{ph} \leq 20$	7.6
LS pole pitch (ls_{pp})	$0.7 \leq ls_{pp} \leq 0.9$	0.9
MP height (mp_h) (mm)	$10 \leq mp_h \leq 30$	10
MP pitch (mp_p)	$0.3 \leq mp_p \leq 0.7$	0.65
HS rotor height (hs_h) (mm)	$20 \leq hs_h \leq 50$	24
HS pole height (hs_{ph}) (mm)	$4 \leq hs_{ph} \leq 20$	12
HS pole pitch (hs_{pp})	$0.5 \leq hs_{pp} \leq 0.9$	0.75
Air gap length (mm)	2	–
Objective: Maximize ()	-	–
HS torque (T_{HS}) (Nm)	$T_{HS} \geq 50$	52.4
Torque density (T_d) (kNm/m^3)	-	105

Table IV. Performance of the optimized MGPM machine at rated condition (decoupled)

Performance parameters	Values
Torque density (gear part) (kNm/m^3)	105
Phase current (rms) (A)	6.92
Phase voltage (rms) (V)	213.6
Input power (W)	4457
Output power (W)	4125
Total loss (W)	332
Power factor	0.93
Efficiency	92.55%

Fig. 12. Forces distribution on the shaft

Fig. 13. Deformation analysis of the shaft

Fig. 14. Stepped lamination stack supported by stainless steel rod forming a modulator spoke
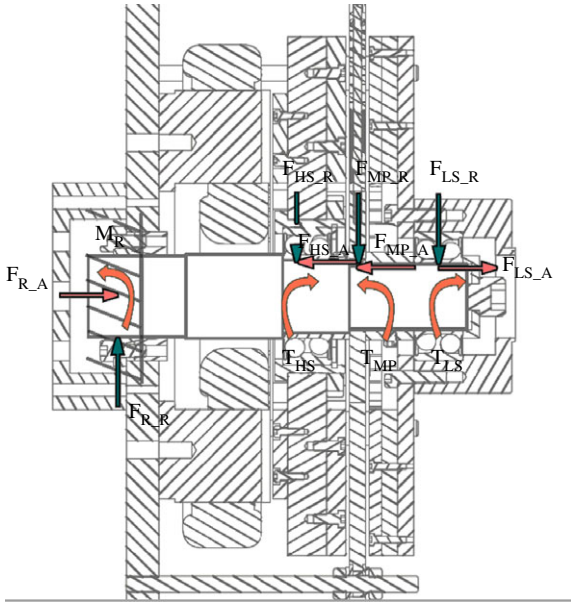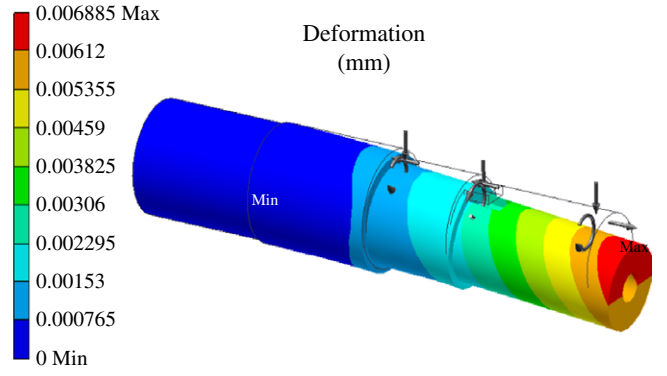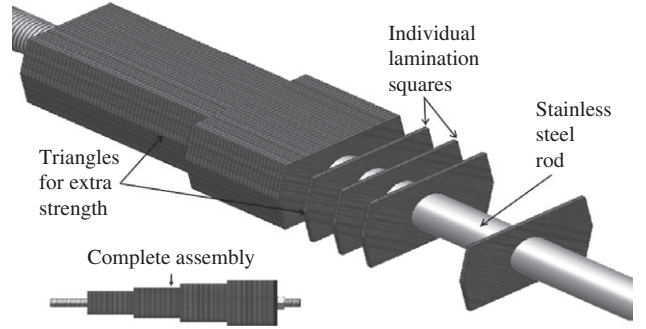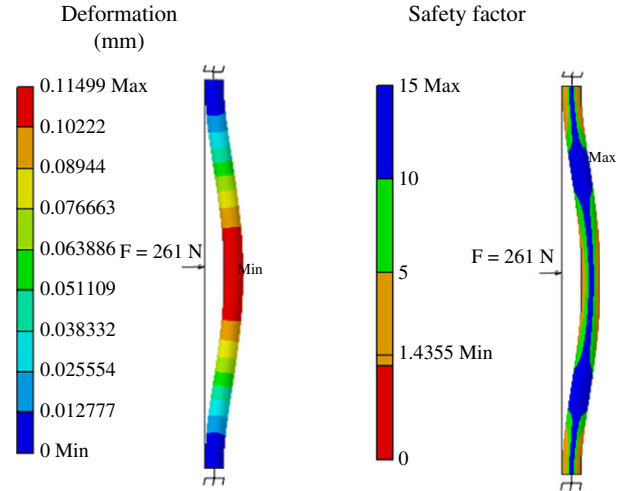

Fig. 15. Deformation and safety factor analysis of a stainless steel supporting rod

and integrity considerations. Various forces resulting from the electrical interaction, the mechanical interaction, and the component mass need to be considered to investigate the strength and reliability of the MGPM machine. It can be seen from Fig. 1 that the stator and the flux modulator are stationary and the LS and HS rotors rotate.

To reduce the number of bearings required, it was decided to keep the shaft stationary. Figure 12 illustrates the forces that the shaft will endure. The radial force components are mainly due to the weight of the different components, while the axial forces and the torque are due to electromagnetic forces.

As shown in Fig. 13, a stress analysis is performed to determine the deformation of the shaft. The maximum deformation is less than 7μm and the safety factor is calculated as 8.7. This means that the shaft is rigid enough for the application. To handle strong axial attraction forces, sealed double-row angular contact ball bearings are used, which provide stability and strength in both axial and radial directions.

To realize both magnetically decoupled and coupled configurations in the same machine, a solid iron disk is used as the PMs carrier, on which the two layers of PMs are arranged either in the same or opposite polarity by mechanically shifting them 60 degrees out of phase.
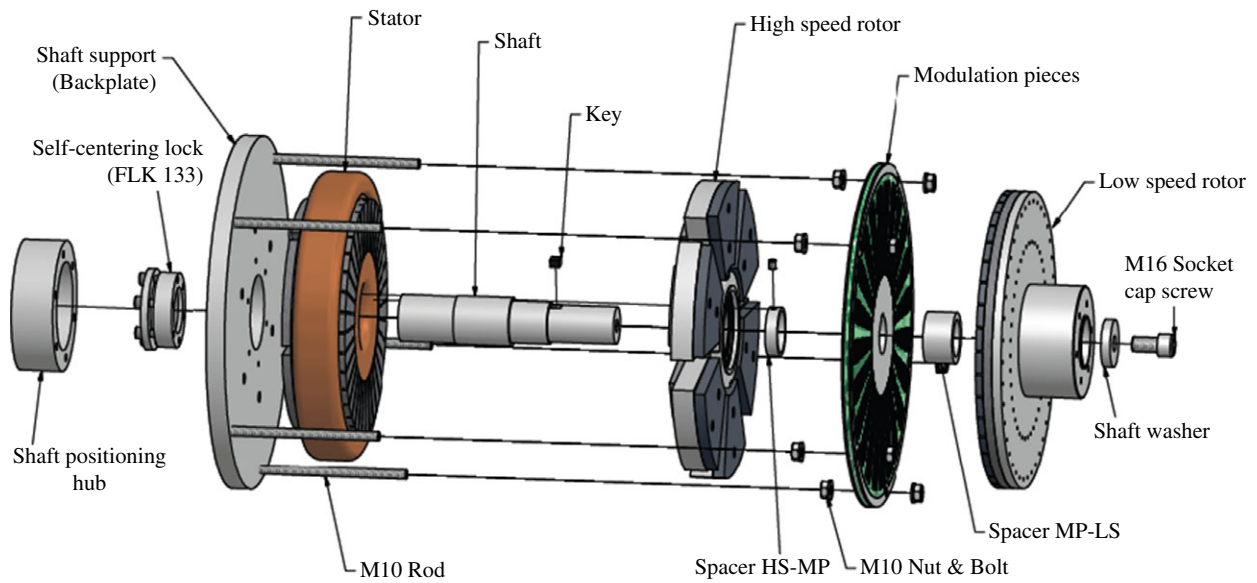
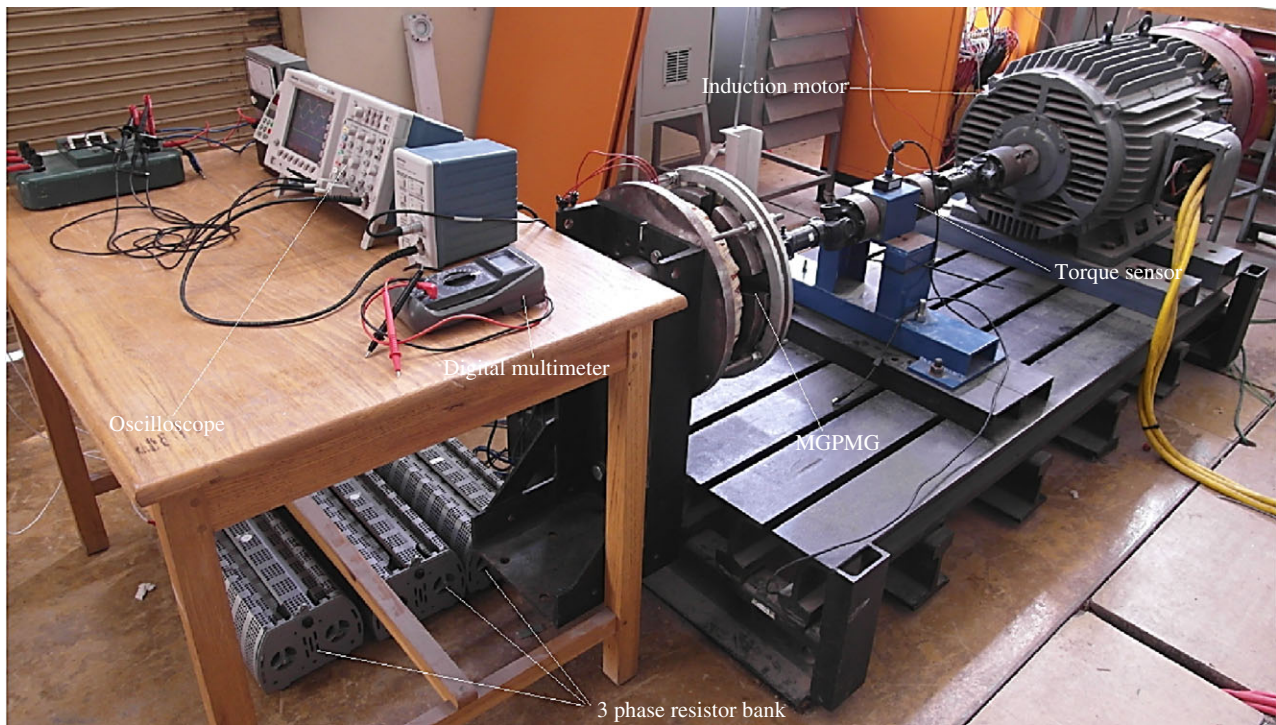Fig. 16. Exploded view of the complete machine

Fig. 17. Test setup for the axial flux MGPM machine

The flux modulator is made from laminated steel to reduce core loss. To simplify the manufacturing process, laser-cut laminations were stacked together to form a modulation spoke. To approximate an annular profile of the spoke, a stepped spoke structure with four sizes of lamination was used, as illustrated in Fig. 14. Stainless steel support rods were also installed to strengthen the structure. The stress analysis shows that the rods have a safety factor of 1.4 and a maximum deformation of 0.115 mm in the middle of the rods, as shown in Fig. 15.

The laminated LS rotor core increases the complexity of mechanical design, as it needs additional support. From the stress analysis, it is found that with a 10 mm steel back plate a safety factor of 2.2 can be achieved. The maximum deformation of 0.22 mm occurs at the disk's outer periphery. The exploded view of the complete machine assembly is shown in Fig. 16.

5. Experimental Evaluations

Figure 17 shows the experimental test setup for the prototype MGPM machine. A four-pole variable speed induction motor drive is used as prime mover, which is connected to the low-speed rotor of the MGPM machine via a Lorenz torque sensor.

The simulated and measured open-circuit voltage waveforms of the axial flux MGPM machine (for both decoupled and coupled configurations) are compared in Fig. 18. The predicted results correlate well with the measurements for the coupled configuration. However, for the decoupled configuration, the predicted result is about 7% lower than the measured one. This is also evident in Fig. 19, which compares the measured and calculated no-load EMF versus speed. Owing to the strong magnetic pulling forces, it is rather difficult to control the exact length for each air gap within the machine. The discrepancy in the results (for the decoupled
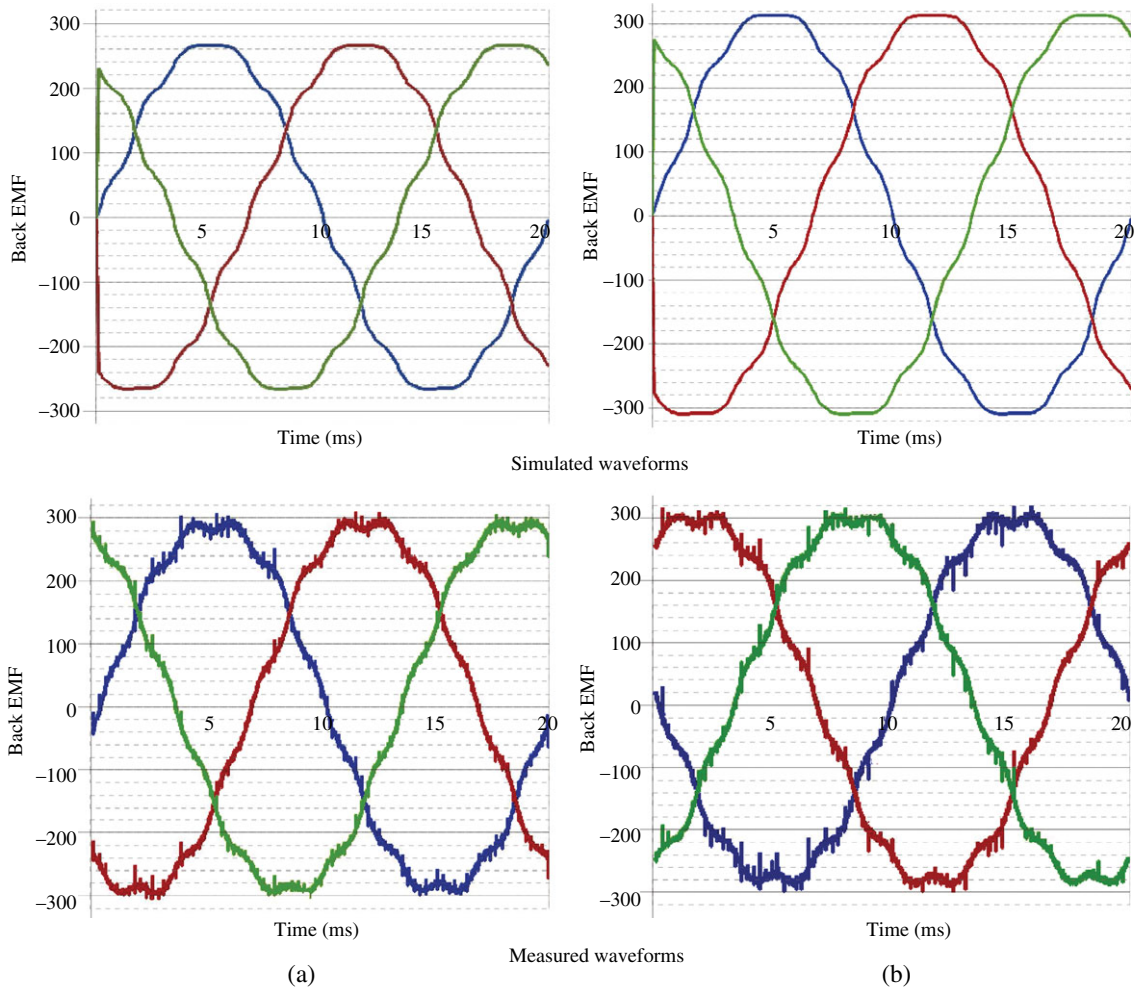
Fig. 18. Comparison of predicted and measured no-load voltage waveforms at rated speed. (a) Decoupled. (b) Coupled
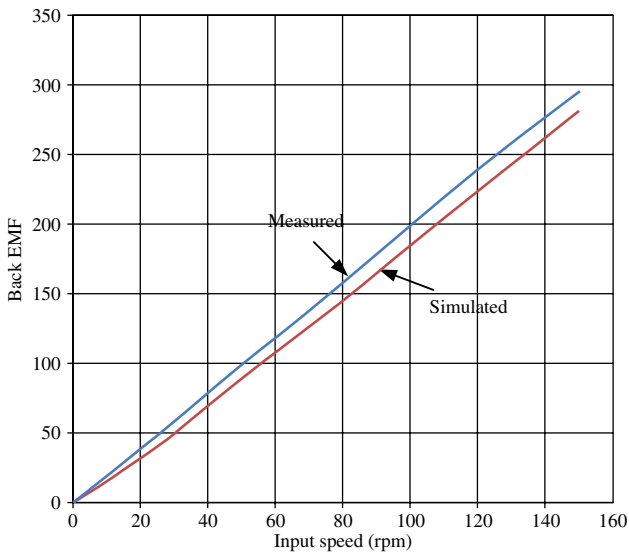

Fig. 19. Comparison of predicted and measured no-load voltage versus speeds (decoupled)

Fig. 20. Measured pull-out torque with HS rotor locked

configuration) is likely because the realized air gap length between the high speed rotor and stator is smaller than the designed one, resulting in a slightly higher air gap flux density. For the coupled configuration, magnetic fluxes go through all air gaps so that the flux linkage to the stator is less sensitive to the small variation of a single air gap length.
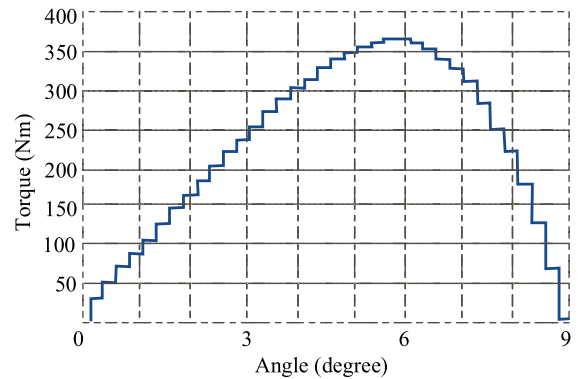
To determine the static pull-out torque of the gear part, the locked HS rotor test is also conducted. As shown in Fig. 20, the measured pull-out torque is about 360 Nm.

To evaluate the dynamic response of the MGPM machine under overload condition, an increasing load is applied to the machine until the gear part of the machine starts to slip. As a safety precaution, the air gaps of the MGPM machine were increased to 4 mm, which reduces the peak torque capability to 200 Nm. Figure 21 displays the measured input torque versus time, in which it can be seen that the gear starts to slip just under 200 Nm. After the slip point, the MGPM machine oscillates at a high frequency until the input speed is brought down to stand still. This is clearly an evidence of overload protection.
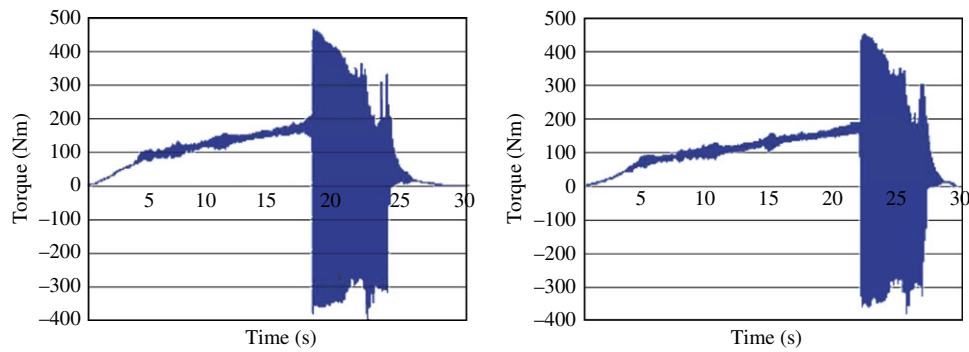
Fig. 21. Test to demonstrate the overload protection of the prototype machine. (a) Decoupled. (b) Coupled

To regain the magnetic gearing action, the LS rotor needs to start from an equilibrium position. For wind power applications, a pole-slipping detection and recovery system would be essential to restore the power transfer after an overload condition. It is observed that the MGPM with coupled configuration settles faster than the decoupled one. This may be attributed to the additional damping effects from the stator. Unlike the decoupled configuration, which requires a thick yoke for the HS rotor to separate the fluxes of the gear and the stator, the coupled one has the advantage that it requires no yoke for the HS rotor, resulting in a shorter axial length of the machine. For wind generator applications, the coupled design may be preferred because of its higher torque density. However, the relatively low inductance of the machine in the coupled configuration suggests that the decoupled configuration may be more suited to certain applications (e.g. traction application).

6. Conclusion

In this paper, a novel axial flux MGPM machine for wind power application was described. The design procedure, mechanical construction, and experimental evaluation of the machine for both magnetically coupled and decoupled configurations were presented. The optimized results show that a torque density over $100\,kNm/m^3$ can be achieved for the active gear part, which is comparable with that of typical mechanical gears such as spur gears ($100-200\,kNm/m^3$) and two- to three-stage helical gears ($50-150\,kNm/m^3$). The inherent overload protection of the MGPM machine has also been demonstrated, which is a clear advantage for wind power application comparing with mechanical gears. Given the complex structure of the axial flux MGPM machine, mechanical strength and integrity considerations are essential in the design of these machines. The design optimization shows that for an integrated axial flux magnetically geared PM machine, to match the torque capability between the magnetic gear and PM machine, the diameter of the gear part tends to be larger than that of the machine part. This implies that the radial flux configuration, where a PM machine fits inside a magnetic gear, would be inherently more suited for MGPM machines.

Acknowledgment

References

(1) Ragheb A, Ragheb M. Wind turbine gearbox technologies, Proceedings of the 1st International Nuclear and Renewable Energy Conference (INREC10), 2010.

(2) Wang R-J, Gerber S. Magnetically geared wind generator technologies: opportunities and challenges. *Applied Energy* 2014; **136**: 817−826.

(3) Atallah K, Howe D. A novel high-performance magnetic gear. *IEEE Transactions on Magnetics* 2001; **37(4)**:2844−2846.

(4) Chau K, Zhang D, Jiang J, Lui C, Zhang Y. Design of a magnetic-geared outer-rotor permanent-magnet brushless motor for electric vehicles. *IEEE Transactions on Magnetics* 2007; **43**:2504−2506.

(5) Atallah K, Rens J, Mezani S, Howe D. A novel pseudo direct-drive brushless permanent magnet machine. *IEEE Transactions on Magnetics* 2008; **44(11)**:4349−4352.

(6) Rasmussen P, Jahns T, Toliyat H, Mortensen H, Matzen T. Motor integrated permanent magnet gear with a wide torque-speed range. IEEE Energy Conversion Congress and Exposition, ECCE, 2009.

(7) Jian L, Chau K, Jiang J. An integrated magnetic-geared permanent-magnet in-wheel motor for electric vehicles. IEEE Vehicle Power and Propulsion Conference (VPPC), 2008.

(8) Jian L, Chau K. Design and analysis of an integrated halbach−magnetic-geared permanent-magnet motor for electric vehicles. *Journal of Asian Electric Vehicles* 2009; **7(1)**:1213−1219.

(9) Jian L, Chau K, Jiang J. A magnetic-geared outer-rotor permanent-magnet brushless machine for wind power generation. *IEEE Transaction on Industry Applications* 2009; **45(3)**:954−962.

(10) Frank N, Toliyat H. Gearing ratios of a magnetic gear for wind turbines. IEEE International Electrical Machines and Drives Conference, IEMDC09, 2009.

(11) Zhu ZQ, Howe D. Influence of design parameters on cogging torque in permanent magnet machines. *IEEE Transactions on Energy Conversion* 2000; **15**:407−412.

(12) Hassan R, Cohanim B, de Weck O, Venter G. A comparison of particle swarm optimization and the genetic algorithm. 46th AIAA/ASME/ASCE/AHS/ASC Structures, Structural Dynamics and Materials Conference, Texas, 2005; 13 pp.

(13) Wang R-J, Kamper MJ, Van der Westhuizen K, Gieras JF. Optimal design of a coreless stator axial field permanent magnet generator, *IEEE Transactions on Magnetics* 2005; **41(1)**:55−64.

(14) Gerber S, Wang R-J. Design of a magnetically geared PM machine. IEEE International Conference on Power Engineering, Energy and Electrical Drives (POWERENG), Istanbul, 2013; 852−857.

Rong-Jie Wang (Non-member) received his M.Sc. Eng. degree from the University of Cape Town, South Africa, in 1998, and the Ph.D. degree from Stellenbosch University, South Africa, in 2003. He is currently an Associate Professor with the Department of Electrical and Electronic Engineering, Stellenbosch University. His research interests include computer-aided design and optimization of electric machines, computational electromagnetics, and thermal modeling of electrical machines. He has published/presented many research papers in journals/ conferences. He was a co-author of the monograph *Axial Flux Permanent Magnet Brushless Machines* (2nd ed., Springer 2008).

Lodewyk Brönn (Non-member) received the B.E. degree in Mechatronic Engineering in 2009 and the M.Sc. Eng. degree in Electrical Engineering in 2012, both from the Stellenbosch University, South Africa. He is currently an electrical machine design engineer with Adventure Power, East London, South Africa. His research interests include the design of magnetically geared electrical machines for renewable energy applications.

Stiaan Gerber (Non-member) received the B.E. (cum laude) degree in Electrical and Electronic Engineering with computer science from Stellenbosch University, South Africa, in 2008, and the M.Sc.Eng. (cum laude) degree in 2011. He is currently pursuing the Ph.D. degree in the field of electrical machines, with specific focus on magnetically geared electrical machines. His main research interests include electrical machine design, numerical optimization, renewable energy power generation, and finite element methods.

Pushman Tlali (Non-member) received the B.E. degree in Electrical and Electronic Engineering from Stellenbosch University, South Africa, in 2012, and the M.Sc. Eng. degree in 2015. He is currently working toward the Ph.D. degree in the field of special electrical machines. His research interests include optimal design of magnetically geared electrical machines for wind power applications.